

HARD DIFFRACTION AT HERA AND THE TEVATRON*

KERSTIN BORRAS

Deutsches Elektronen-Synchrotron Hamburg
DESY, 22603 Hamburg, Germany

(Received January 4, 2005)

The phenomena of diffractive interactions are briefly introduced. Basic ideas for theoretical descriptions are discussed and recent results on the experimental side with interpretations from the theoretical side are presented.

PACS numbers: 13.90.+i, 13.60.-r, 13.85.-t

1. Introduction

The name diffraction in high-energy particle physics originates from the analogy of the concepts in optics with the description of nuclear high-energy scattering physics introduced in the Fifties by Landau, Pomeranchuk, Feinberg *et al.* [1]. In the Born approximation the same equation for the elastic scattering amplitude can be derived from the scattering of a plane wave passing through and around an absorbing disk, resulting in a “diffraction” pattern for hadron–hadron scattering. In the Good and Walker picture [2] diffractively-produced systems of dissociated particles were predicted to have the same quantum numbers as the initial beam particle. This means that only the quantum numbers of the vacuum are exchanged in diffractive interactions. Taking into account possible dissociation of the beam particles, different classes of diffractive events can be distinguished in hadron–hadron scattering: elastic scattering with both beam particles staying intact (Fig. 1), single diffractive dissociation (SD), in which one beam particle dissociates (Fig. 12), double diffractive dissociation (DD) in which both beam particles dissociate and double pomeron exchange (DPE) (Fig. 12).

In the 1960s, one of the mysteries of strong interaction physics was the enormous proliferation of strong interacting particles or hadrons, which in addition, exhibit a striking property: the more massive the particles, the

* Presented at the XXXIV International Symposium on Multiparticle Dynamics, Sonoma County, California, USA, July 26–August 1, 2004.

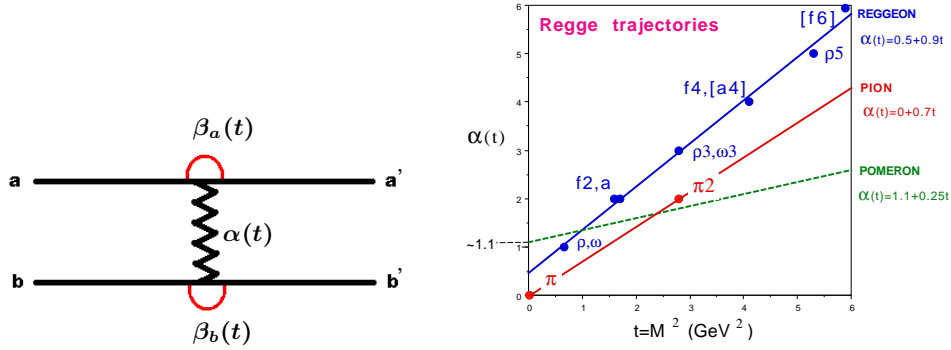


Fig.1. Elastic scattering with the exchange of a Regge trajectory $\alpha(t)$ (left). Schematic Chew–Frautschi plot [3] and the parameterization of the most important Regge trajectories: pion (π), reggeon (R) and pomeron (P) (right).

higher their spin with a linear correlation between the square of the particle mass and its spin (Fig. 1). In Regge Theory [4] this correlation is described in the complex angular momentum plane by linear Regge trajectories: $\alpha(t) = \alpha(0) + \alpha' \cdot t$, which are exchanged between the beam particles as illustrated in the elastic scattering diagram in Fig. 1. In Regge phenomenology diffraction corresponds to the exchange of the pomeron trajectory, which has the quantum numbers of the vacuum. In this framework the total cross section dependence on the center-of-mass energy, \sqrt{s} , is determined by the intercept of the trajectory, $\sim s^{\alpha(0)-1}$, and the elastic and diffractive cross sections are expected to increase with s as $s^{2(\alpha(t)-1)}$, such that the ratio to the total cross section rises with s .

In order to describe the rising behavior of the total cross section the pomeron trajectory was postulated with an intercept of $\alpha_P(0) \approx 1$. In contrast to all other trajectories no particle has been identified on the pomeron trajectory. As the pomeron trajectory has the largest intercept of all Regge trajectories, pomeron trajectory exchanges dominate at high energies and its parameters have been derived from fits to the data of soft diffractive interactions, for example in [5–7]. In Fig. 2 it can be seen that complications arise when applying these parameterizations to even higher energies, where the predictions overestimate considerably the measurements [8]. Different approaches have been developed, for instance by taking into account multiple-pomeron trajectory exchanges in the eikonal approximation [9, 10] or by renormalizing the diffractive cross section parameterization such that the probability for a diffractive interaction to occur does not exceed unity [8, 22].

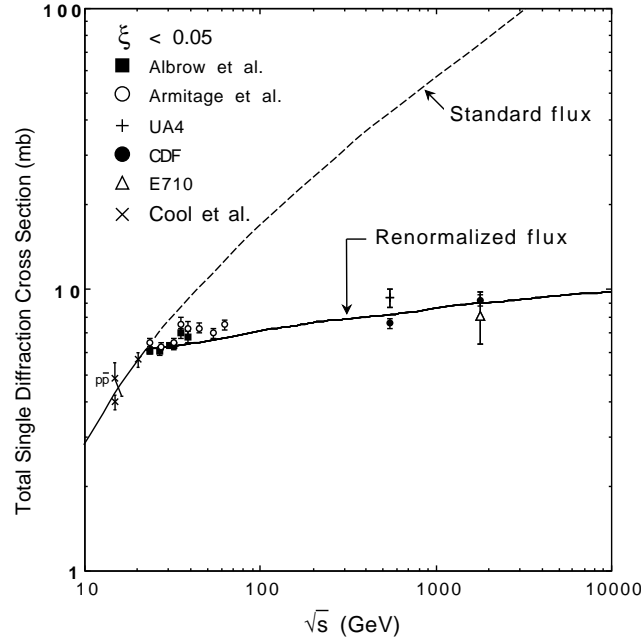


Fig. 2. Measured SD cross section in pp and $\bar{p}p$ scattering as a function of \sqrt{s} compared to standard (dashed) and renormalized [8] predictions from Regge phenomenology.

1.1. Conventions in diffractive scattering

The study of hadronic structures is conveniently performed in deep inelastic scattering (DIS) ep collisions. In Fig. 3 the relevant four vectors for the calculation of the kinematic variables are indicated for diffractive DIS. The virtuality of the photon, Q^2 , reflects the resolving power for probing the structure in the scattering process. The variable x , the Bjorken scaling variable, denotes in the Quark Parton model the longitudinal momentum fraction of the scattered parton with respect to the proton. The longitudinal momentum fraction of the proton carried by the diffractive exchange is usually named x_P , taken from the notion that a pomeron, as a virtual particle on the pomeron trajectory, is exchanged. The variable β is defined relative to the diffractive exchange and gives in the Quark Parton model the longitudinal momentum fraction of the scattered parton relative to x_P . The squared four-momentum transfer at the proton vertex is given by the variable t . Traditionally the quantity x_P is referred to as ξ in hadron-hadron scattering.

From the measured inclusive DIS cross section the proton structure function can be unfolded via: $\frac{d^2\sigma}{dx dQ^2} = \frac{2\pi\alpha^2}{xQ^4} [1 + (1-y)^2] \sigma_r(x, Q^2)$, where σ_r is the reduced cross section and is identical to F_2 in the kinematic regions where F_L can be neglected: $\sigma_r(x, Q^2) = F_2(x, Q^2) - \frac{y^2}{1+(1-y)^2} F_L(x, Q^2)$. The total γ^*p cross section is related to F_2 by: $\sigma_{\text{tot}}(\gamma^*p) = \frac{4\pi^2\alpha}{Q^2(1-x)} F_2(x, Q^2)$.

For diffractive interactions two more kinematic variables are needed to describe the full kinematics: $x_P (= \xi)$ and t . If t cannot be measured because of the selection method applied, the diffractive contribution is integrated over t and the diffractive structure function of the proton is given by: $\sigma_r^{D(3)}(x_P, \beta, Q^2) = F_2^{D(3)}(x_P, \beta, Q^2) - \frac{y^2}{1+(1-y)^2} F_L^{D(3)}(x_P, \beta, Q^2)$.

One possible factorization ansatz for the complex calculations of physics processes in the framework of QCD is the factorization of the cross section into parton density functions and the cross section of the hard subprocess. The QCD factorization theorem is expected to hold also in diffractive DIS [11–13] and conditional diffractive parton density functions can be defined, which should be universal if probed by different processes at the same x_P and t . For photoproduction (PHP) and $\bar{p}p$ collisions this QCD factorization is presumed to be violated [11]. An additional factorization assumption, Regge factorization, decomposes $F_2^{D(3)}$ into a universal pomeron flux $f_{P/p}$ and a universal pomeron structure function F_2^P :

$$F_2^{D(3)}(x_P, \beta, Q^2) \sim f_{P/p}(x_P) F_2^P(\beta, Q^2) \quad \text{with} \quad f_{P/p}(x_P) \sim \frac{1}{(x_P)^{2\alpha_P(t)-1}}.$$

The pomeron flux comprises the soft part of the diffractive interaction and depends only on the diffractive kinematic variables x_P and t , while the pomeron structure function is only a function of the quantities β and Q^2 . Both factorization ansatzes can be tested by experiments in both DIS and PHP in ep collisions and with different processes in $\bar{p}p$ scattering.

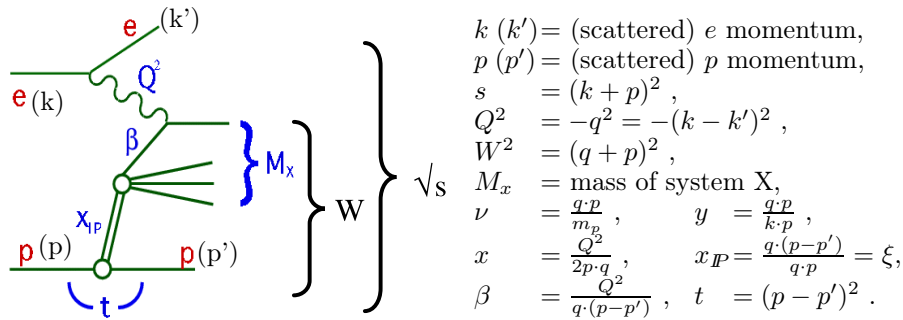


Fig. 3. Kinematic variables at HERA.

Several models for the description of diffractive interactions are available, only some of them are outlined here. One of the most commonly used is the Ingelman–Schlein model [14] which assumes Regge factorization by parameterizing the pomeron flux with cross section dependencies as measured in soft diffractive hadron–hadron scattering. The pomeron structure function is derived by QCD fits based on the DGLAP evolution equations. This ansatz is also known as resolved \mathbb{P} model (see details in [15]).

Another set of models, the color dipole models, employ the fluctuations of the photon into a $q\bar{q}$ or $q\bar{q}g$ color dipole, scattering off the proton via two-gluon exchange (Fig. 4). The cross section for the dipole-proton interaction can be derived from inclusive DIS measurements. Including unitarization effects through saturation (see [17] for more details) leads to a good description of the data [19]. In this framework diffractive exchanges possess no universal nature, but depend on the type of process.

Simultaneous QCD fits to F_2 and $F_2^{D(3)}$ have been used in a model [16], in which the diffractive exchange is represented by the exchange of two gluons or two sea quarks. By relating the pomeron flux back to the proton parton density functions of gluons and sea quarks at the relevant scale for the scattering, these fits do not assume Regge factorization.

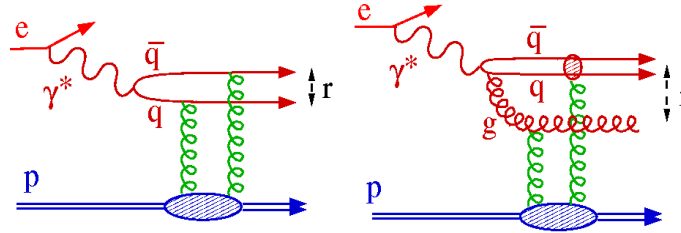


Fig. 4. Schematic drawing of diffractive interactions in color dipole models in lowest order.

Soft color interactions between the partons, as implemented in Monte Carlo simulations [20], have also been successful in the reproduction of the measurements. The diffractive interaction (or an effective pomeron exchange) is in this case not an intrinsic part of the proton, but a dynamical effect of the interaction. The framework of parton re-scattering processes provide a theoretical basis [21] for the soft color interaction model.

A phenomenological approach is taken in the Deep Sea model [22], in which the asymptotic dependence of the proton parton density functions for gluons and quarks in the sea region at small x are used at low Q^2 to derive the essential parameters for the soft diffraction dependencies and at higher Q^2 to predict relations for hard diffraction, for instance between F_2 and $F_2^{D(3)}$ which can be compared to measurements [22].

2. Measurements at HERA

Diffractive events can be selected at HERA by different methods: either by directly measuring the leading proton [25,26] or by requiring the presence of a rapidity gap [24], which is a natural consequence of the kinematics of diffractive events. The M_X method [23] can also be employed to determine the diffractive contribution on a statistical basis. The result of the three different methods differ by the contribution from proton dissociation and non-diffractive interactions like, for example, \mathbb{R} exchanges.

The ratio of the diffractive cross section to the total cross section has been measured in different M_X ranges and for various values of Q^2 as a function of W (Fig. 5). The diffractive contribution, as determined by the M_X method, is approximately independent of W , which is in clear contrast to the expectation from Regge phenomenology as the total cross section is predicted

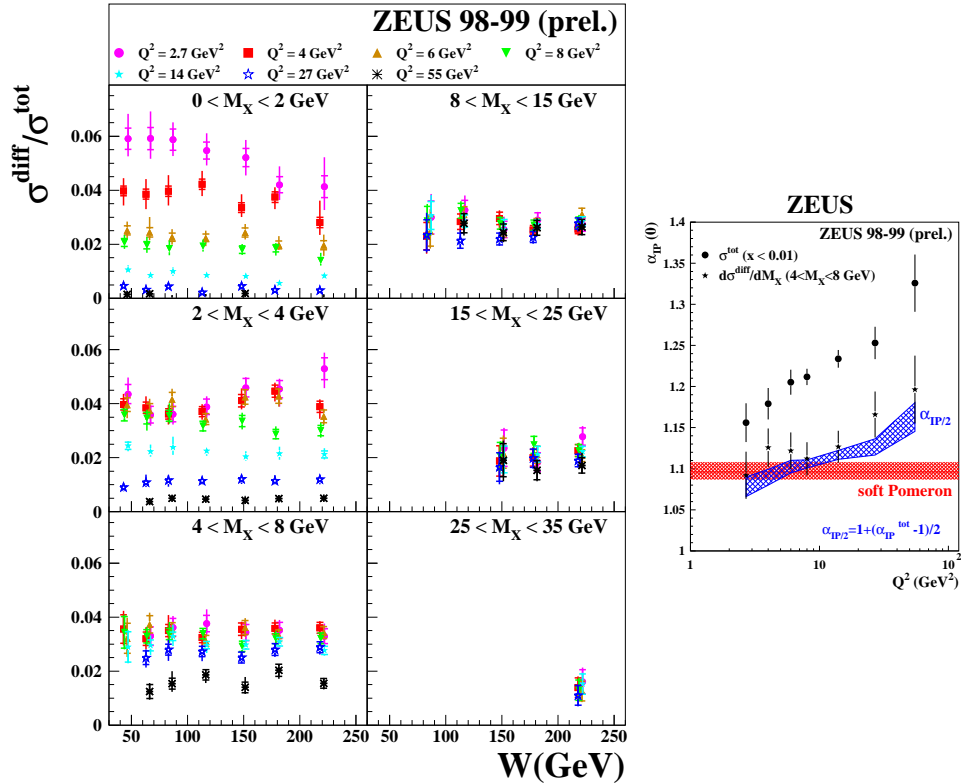


Fig. 5. Ratio $\sigma^{\text{diff}}/\sigma^{\text{tot}}(Q^2)$ as a function of W (left), $\alpha_P^{\text{diff}}(0)$ as a function of Q^2 , compared to $\alpha_P^{\text{tot}}(0)$ (right). The horizontal line indicates the value of $\alpha_P(0)$ derived from soft diffractive hadron-hadron scattering and the band marks its uncertainty [23].

to rise as $(W^2)^{\alpha_P(0)-1}$ and the diffractive contribution as $(W^2)^{2(\alpha_P(t)-1)}$. The values of $\alpha_P(0)$ were derived separately from each set of measurements (Fig. 5) and the nearly constancy in the W dependence translates into a factor of approximately two difference in $\alpha_P(0)$ between the total cross section measurements and the diffractive cross section. In the framework of Regge phenomenology, no Q^2 dependence is expected for $\alpha_P(0)$. Within the experimental uncertainties of the diffractive measurements the tendency to rise with Q^2 can be approximated by one average value for $\alpha_P(0)$, which turns out to lie significantly above the $\alpha_P(0)$ value extracted from soft diffractive hadron-hadron interactions. All these results are indications that the parameters for a (universal) pomeron trajectory as derived from soft diffraction measurements cannot be applied directly to hard diffraction as well. The flat behavior of the ratio $\sigma^{\text{diff}}/\sigma^{\text{tot}}$ is built-in, for example, in the dipole saturation model [19] and the Deep-Sea model [22].

The inclusive diffractive DIS cross section measurements have been used to unfold the diffractive structure function of the proton and $x_P \sigma_r$ is shown in Fig. 6 for diffractive data selected by requiring a rapidity gap or a leading proton. The large amount of data and the high precision have been used to extract diffractive parton density functions assuming Regge factorization with one averaged $\alpha_P^{\text{diff}}(0)$ determined simultaneously in the QCD fits to the selected diffractive events (see details in [15]). The line in Fig. 6 demonstrates the good description of the data within the experimental uncertainties. An equally good description is possible with the color dipole models, for example the BEKW model [18], which is shown in Fig. 7 [23]. This figure displays $x_P F_2^{D(3)}$ as derived from measurements using the M_X method.

The large data sets available up to now have even allowed the observation of charged current events with a rapidity gap at high Q^2 ($> 200 \text{ GeV}^2$) [33, 34]. In total nine events were identified and the data distributions have been found to be consistent with expectations obtained by MC simulations employing diffractive parton density functions [33]. The extracted diffractive parton density functions are also used to predict cross sections for the production of some hadronic final states (see details in [15]). As expected from QCD factorization, diffractive dijet and D^* production in DIS can be well described by these diffractive parton density functions. In diffractive PHP a factor of approximately two discrepancy is observed, not only for the resolved photon contribution, but also astonishingly for the direct photon contribution. It is also noteworthy that in the related case of leading baryon production factorization violation is visible in inclusive measurements of the transition from PHP to the DIS regime (Fig. 9) [28, 30] and in associated dijet production [29].

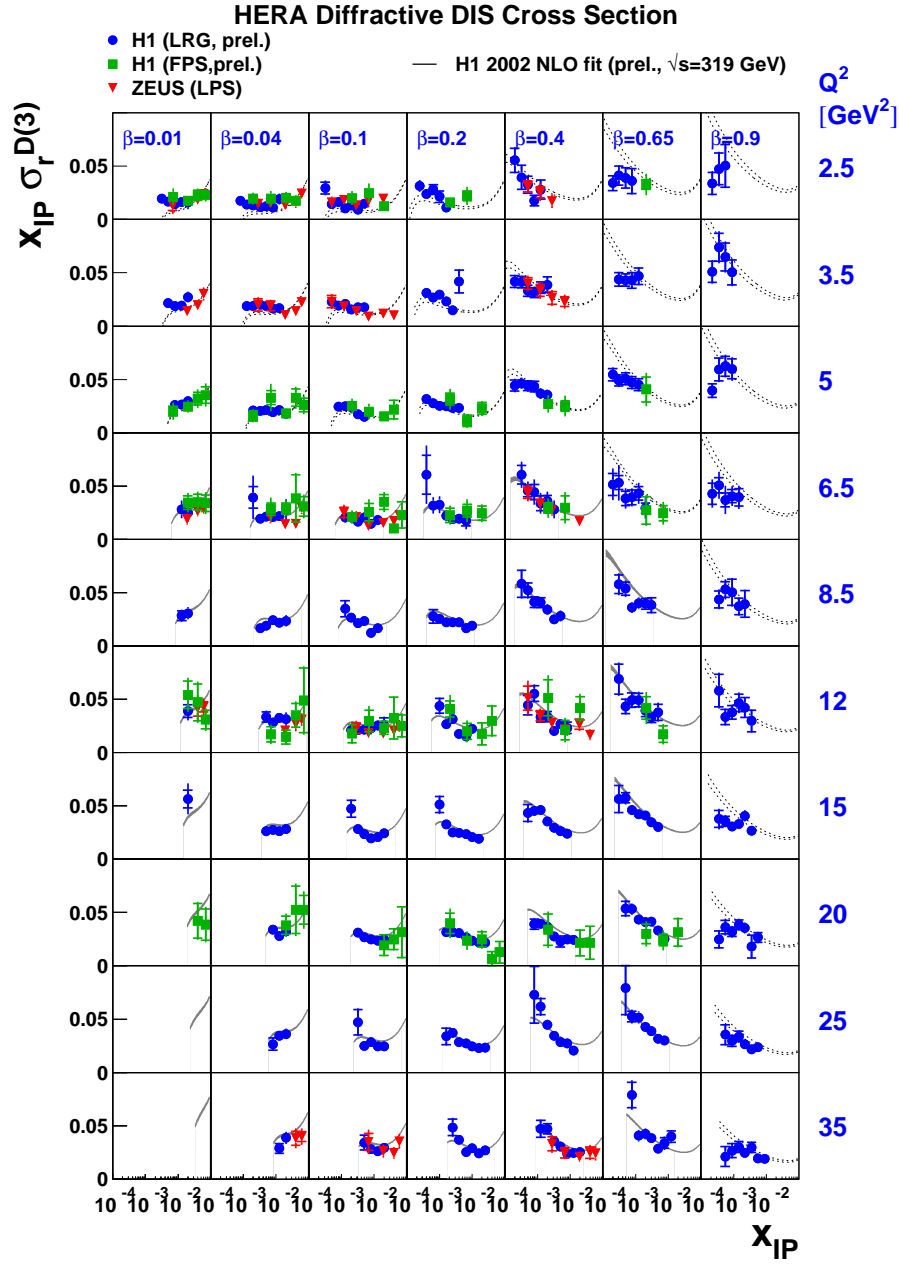


Fig. 6. Diffractive structure function measurements from H1 [24,25] and ZEUS [26]. The line denotes the result of a QCD fit performed by the H1 Collaboration [27].

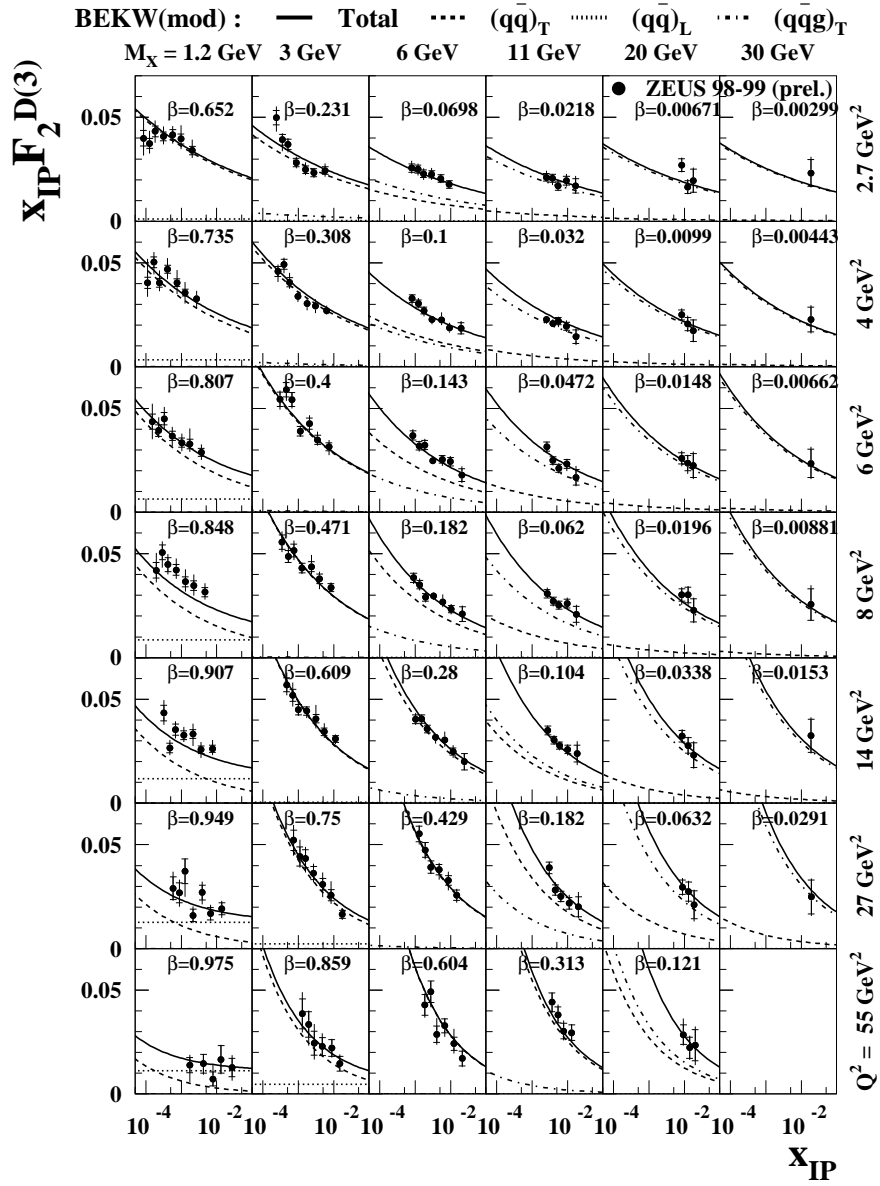


Fig. 7. Diffractive structure function measurements compared to a fit with the BEKW model [23].

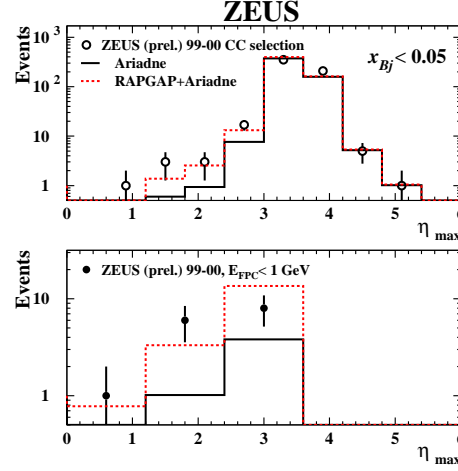


Fig. 8. Distribution of the quantity η_{\max} (a measure of the size of the rapidity gap) for charged current DIS events with $Q^2 > 200 \text{ GeV}^2$. Data are compared to non-diffractive (solid line) and to diffractive plus non-diffractive (dashed line) MC simulations in the upper plot. The lower plot shows the comparison when a diffractive selection cut is applied. The cross sections derived from these measurements are [33]: $\sigma_{cc}^{\text{diff}} = 0.49 \pm 0.20(\text{stat.}) \pm 0.13(\text{syst.}) \text{ pb}$, $\frac{\sigma_{cc}^{\text{diff}}}{\sigma_{cc}^{\text{tot}}} = 2.9 \pm 1.2(\text{stat.}) \pm 0.8(\text{syst.})\%$.

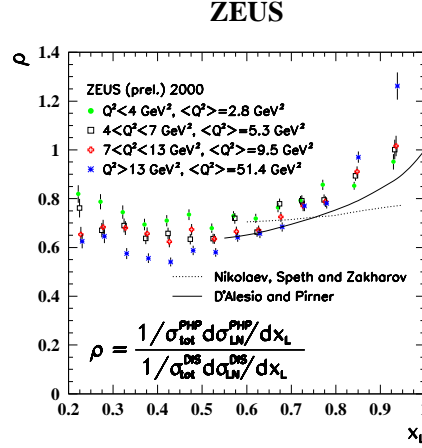


Fig. 9. Ratio of leading neutron production rate in PHP and DIS for four different ranges of Q^2 as a function of $x_L = 1 - x_P$ [30]. The curves represent predictions from two different absorption models. The solid line denotes calculations for initial and final state interactions by additional pomeron exchange [31], the dotted line accounts for a possible destruction of the residual neutron by the projectile during target fragmentation [32].

3. Measurements at the Tevatron

Tests of QCD factorization can be performed at the Tevatron by comparing different processes such as dijet production to J/ψ production [35] or dijet production at different center-of-mass energies [36] or in SD and DPE interactions [37]. A comparison between HERA and Tevatron data can be carried out by predicting diffractive dijet production at the Tevatron using diffractive parton densities derived from HERA measurements. At leading order an effective structure function for dijet production can be defined as $F_{jj} \sim x[g(x) + 4/9 \sum (q(x) + \bar{q}(x))]$, which can be unfolded from the ratio of diffractive to non-diffractive dijet production $R_{ND}^{SD}(x) \sim F_{jj}^D/F_{jj}$ by multiplying it with F_{jj} as calculated from parameterizations of the proton parton density functions. The comparison with the expectations from the diffractive parton densities determined by the H1 Collaboration shows a discrepancy of the order of a factor of 10 (Fig. 10, left) [27, 38]. Using earlier published ZEUS measurements for the determination of the diffractive parton densities via QCD fits, a smaller discrepancy is observed [39], which is confirmed by QCD fits to the recently published ZEUS data [40].

While the H1 measurements were performed for $x_P < 0.05$, the CDF data were taken in the range of $0.035 < x_P < 0.095$, suggesting a substantial contribution from \mathbb{R} or even π exchanges in the data sample. A way to

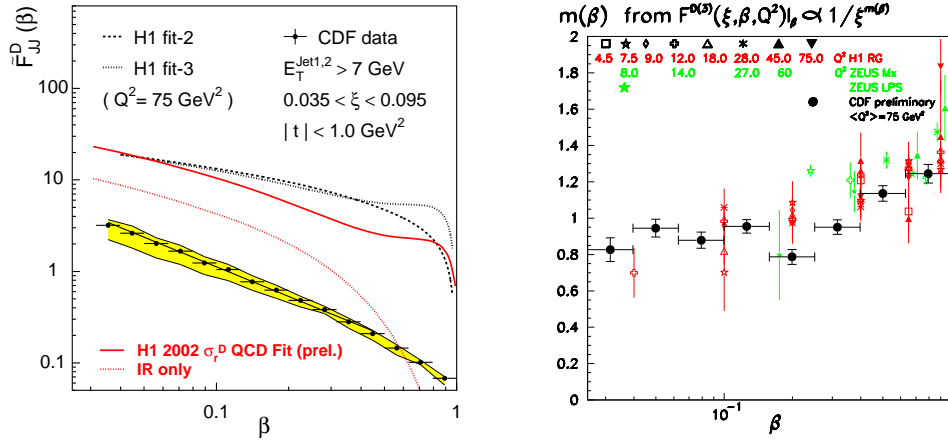


Fig. 10. Left: Diffractive structure function, F_{jj}^D , for dijet production as measured by the CDF Collaboration in $p\bar{p}$ collisions [38]. The curves represent predictions for F_{jj}^D as derived from published and preliminary diffractive parton densities [27, 41]. The contribution from additional Reggeon exchanges from the preliminary parameterization is also indicated. Right: Power m from a power law fit to the $x_P (= \xi)$ dependence of the diffractive structure function $F^{D(3)}(x_P, \beta, Q^2)|_\beta \sim 1/(x_P)^m$ derived from the CDF dijet data and from HERA DIS data.

test the influence of possible \mathbb{R} or π exchanges in the CDF data is given by the analysis of the $x_P(=\xi)$ dependence, which was performed with a power law fit $\sim 1/(x_P)^m$ to the data (Fig. 10, right). According to Regge phenomenology the power m would be expected to be $m_P \approx 1.1$ for pomeron exchanges, $m_R \approx -0.2$ for reggeon exchanges and $m_\pi \approx -1.2$ for pion exchanges. The CDF dijet data reveal only positive values for m close to m_P , proving the dominance of diffractive (\mathbb{P}) exchanges in the selected events. In addition the $x_P(=\xi)$ dependence analyzed as a function of β exhibits the same behavior as extracted from diffractive DIS data selected with the three different selection methods at HERA [41–43].

The available dijet data sample has grown considerably with the arrival of data from Run II [44]. The left plot in Fig. 11 demonstrates the independence of the ratio on $x_P(=\xi)$, which means that the diffractive structure function F_{jj}^D stays the same when going from the low x_P regime in which \mathbb{P} exchanges dominate to high x_P values where strong contributions from \mathbb{R} or even π exchanges would be expected. The independence of the ratio on Q^2 as given by different jet E_T regions (Fig. 11, right) indicates that the evolution of the diffractive structure function F_{jj}^D is similar to that of the proton.

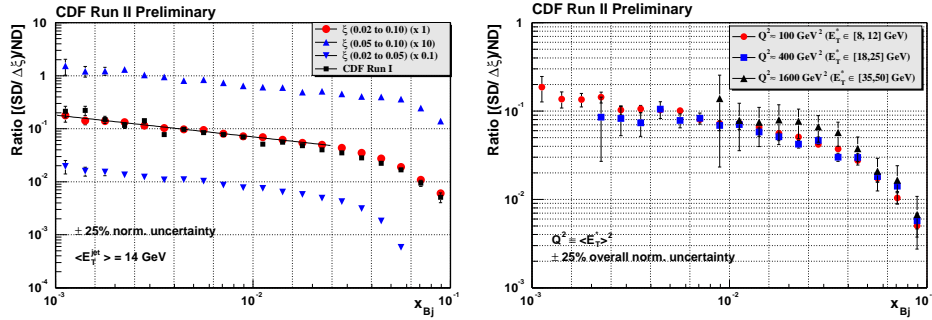


Fig. 11. Ratio of diffractive to non-diffractive dijet production as a function of x for different ranges of $x_P(=\xi)$ and Q^2 [44].

Another factorization test within the Tevatron data can be performed by using single diffractive and DPE events. If factorization holds then the ratio $R_{\text{ND}}^{\text{SD}}(x)$ on the anti-proton side should be the same as the ratio $R_{\text{SD}}^{\text{DPE}}(x)$ on the proton side (left plot in Fig. 12). However a discrepancy of a factor of approx. 5 is revealed in the right hand plot in Fig. 12 indicating again that factorization is broken. The extracted F_{jj}^D is in relatively good agreement with the one expected from HERA [44, 45]. This result is compatible with the assumption that additional gaps should be free from any survival probability [22] as observed in recent measurements of soft diffractive interactions by the CDF Collaboration [45].

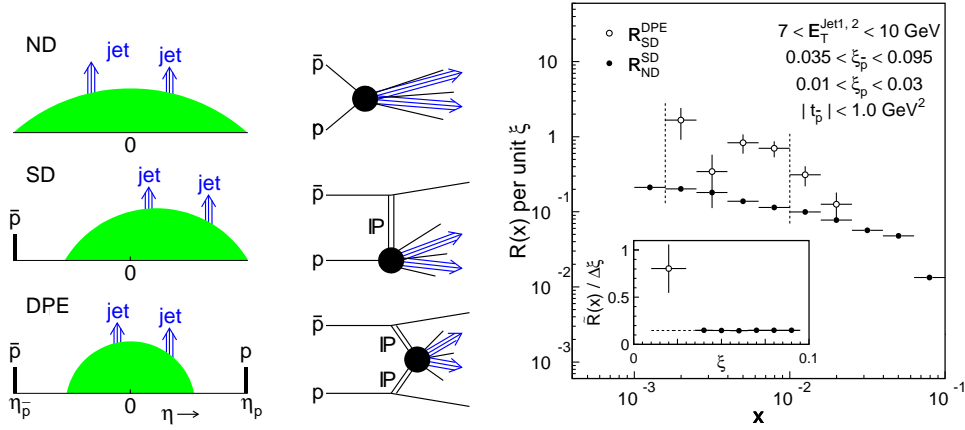


Fig. 12. Schematic picture of event topologies in non-diffractive (ND) and single diffractive (SD) dijet production compared to double pomeron exchange (DPE) (left). Ratios of dijet production in non-diffractive, single diffractive dissociation and double pomeron exchange events as a function of x and $x_P (= \xi)$ (right) [37].

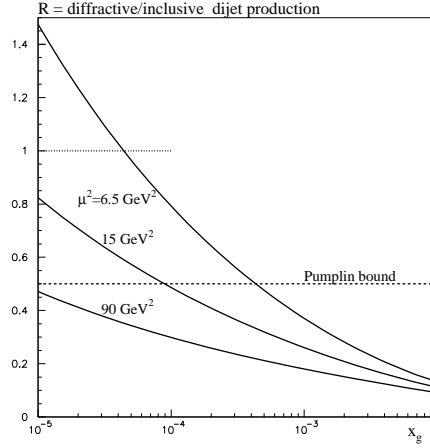


Fig. 13. Predictions for the ratio of diffractive to inclusive dijet production as a function of x_{gluon} for different scales μ^2 calculated with $x_P^{\max} = 0.1$ [9]. The dashed line denotes the unitarity limit called Pumplin bound, which states that $\sigma^{\text{diff}}/\sigma^{\text{tot}} < 0.5$ [49].

A large effort is underway on the theoretical side to model the gap survival probability, which is an important ingredient to estimate the cross section for a prominent discovery channel at the LHC, namely diffractive Higgs production in DPE [46]. Several aspects of factorization breaking in terms of gap survival probability are reproduced by different approaches (see for

example [22] and models employing multi-pomeron exchanges in the eikonal approximation [9, 47]). Exclusive dijet and χ_c production at the Tevatron studied by the CDF Collaboration [44, 45] are excellent testing grounds for these Higgs production calculations. Predictions for diffractive dijet production in PHP and DIS at HERA can also be calculated within this model [48] and reveal unitarity effects occurring even in moderate kinematic regions, which are strongly related to the gluon density function (Fig. 13). Another way to explore such effects and hence to probe the gluon density is given by the study of exclusive (diffractive) vector meson production.

4. Exclusive vector meson production at HERA

Two approaches to the description of vector meson (VM) production in ep collisions are illustrated in Fig. 14. Within the vector dominance model (VDM) the process can be viewed as a fluctuation of the photon into a vector meson (ρ , ϕ or ω), which subsequently scatters diffractively on the proton (left plot). Using Regge phenomenology the cross section can be described as the convolution of the probability for the photon to fluctuate into the VM and the cross section $\sigma(\text{VM } p \rightarrow \text{VM } p)$, which is expected to result in an approximate $W^{0.22}$ dependence. Using the t dependence of the differential cross section $d\sigma/dt \sim W^{4(\alpha_P(t)-1)}$ the parameters of the pomeron trajectory can be unfolded.

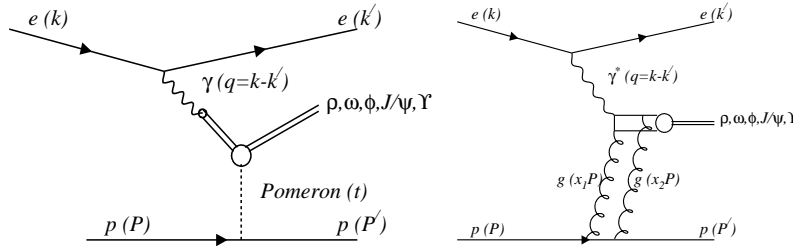


Fig. 14. Models for vector meson production in ep collisions at HERA (see text for explanation).

Within two-gluon exchange models (Fig. 14, right), small $q\bar{q}$ dipole configurations can be calculated using pQCD. In such models the cross section is directly connected to the gluon density of the proton: $\sigma(\gamma^* p \rightarrow \text{VM } p) \sim 1/Q^6 [xg(x, Q^2)]^2$. The increase of the gluon density for small x (or equivalently large W), leads to a strong increase of the cross section with W ($W^{0.8}$) and to a Q^2 dependence which is milder than $1/Q^6$. The t dependence is expected to be universal and exponential, $\sim e^{bt}$, with $b_{2g} \approx 4 \text{ GeV}^{-2}$. Only a small slope $\alpha'_P \approx 0$ is expected. The small dipole size configuration is dominant in processes with longitudinal polarized photons, γ_L^* , and the production of heavy VM like the J/ψ .

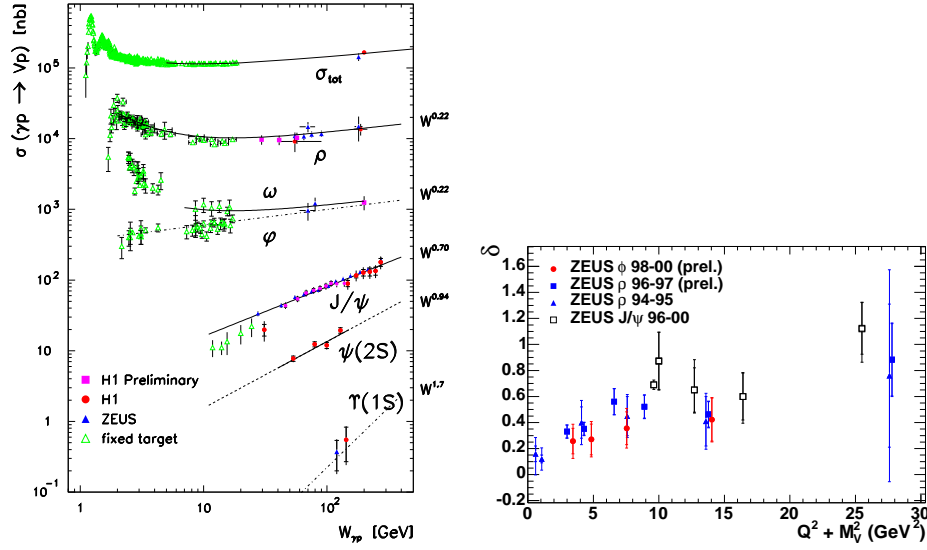


Fig. 15. Cross section for VM production in PHP as a function of W (left). Dependence of the power δ in a power law behavior $\sim W^\delta$ in DIS as a function of $Q^2 + M_{VM}^2$ [50].

The left plot in Fig. 15 displays the W dependence of the PHP production cross sections for different VMs and reveals for the light VMs a behavior expected from VDM+Regge, while for heavier VMs the involved scale becomes hard and the dependence expected from pQCD calculations becomes visible. The production of VMs has been analyzed in the DIS regime and

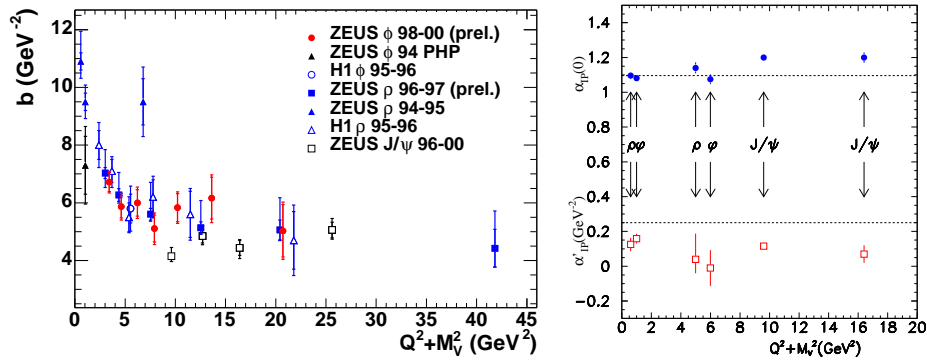


Fig. 16. Dependence of the slope, b , of the exponential t behavior of the VM production cross sections (left) [50] and pomeron trajectory parameters for different VM production processes as a function of $Q^2 + M_{VM}^2$ (right) [51].

the W dependence fitted to a power law $\sim W^\delta$. The power δ is presented in the right hand plot and exhibits a rising behavior which converges to the expected pQCD value with increasing $Q^2 + M_{\text{VM}}^2$ (a measure of the hardness of the scale). The same is true for the extracted b values for assuming an exponential t dependence of the production which converge at large values of $Q^2 + M_{\text{VM}}^2$ to the predicted b_{2g} value (Fig. 16, left). On the right hand side of Fig. 16 the measurements of the pomeron trajectory parameters are compiled for different VM production processes [51] and demonstrate the smallness of α'_p compared to the value of ≈ 0.25 extracted from soft diffractive hadron scattering data.

It is a pleasure to thank my colleagues from the ZEUS, H1 and CDF Collaboration, for their hard work to achieve these important results on diffraction, for helpful discussions during the preparation of this report and last but not least for providing so nice figures to illustrate complicated topics. I am grateful to J. Cole for reading the manuscript. Many thanks to the organizers for this very interesting symposium.

REFERENCES

- [1] V. Barone, E. Predazzi, *High-Energy Particle Diffraction*, Springer-Verlag, 2002, ISBN 3-540-42107-6.
- [2] M.L. Good, W.D. Walker, *Phys. Rev.* **120**, 1857 (1960).
- [3] G.F. Chew, S.C. Frautschi, *Phys. Rev. Lett.* **8**, 41 (1962).
- [4] T. Regge, *Nuovo Cim.* **14**, 951 (1959); *Nuovo Cim.* **18**, 947 (1960).
- [5] A. Donnachie, P.V. Landshoff, *Phys. Lett.* **B296**, 227 (1992) and references therein.
- [6] CDF Collaboration, *Phys. Rev.* **D50**, 5518, 5535, 5550 (1994).
- [7] J. Cudell *et al.*, *Phys. Rev.* **D61**, 034019 (2000); Err. *Phys. Rev.* **63**, 059901 (2001).
- [8] K. Goulianos, *Phys. Lett.* **B358**, 379 (1995); Err. *Phys. Lett.* **363**, 268 (1995).
- [9] V. Khoze, A. Martin, M. Ryskin, *Eur. Phys. J.* **C18**, 167 (2000).
- [10] E. Gotsman *et al.*, *Phys. Rev.* **D49**, R4321 (1994); *Phys. Rev.* **D60**, 094011 (1999); U. Maor, [hep-ph/0406303](#).
- [11] J. Collins, *Phys. Rev.* **D57**, 3051 (1998); Err. *Phys. Rev.* **61**, 019902 (2000).
- [12] A. Berera, D. Soper, *Phys. Rev.* **D53**, 6162 (1996).
- [13] L. Trentadue, G. Veneziano, *Phys. Lett.* **B323**, 201 (1994).
- [14] G. Ingelman, P. Schlein *Phys. Lett.* **B152**, 256 (1985).
- [15] C. Kiesling, *Acta Phys. Pol. B* **36**, 617 (2005) these proceedings.

- [16] A. Martin, M. Ryskin, G. Watt, *Eur. Phys. J.* **C37**, 285 (2004); *Phys. Rev.* **D70**, 091502 (2004).
- [17] J. Bartels, *Acta Phys. Pol. B* **36**, 657 (2005) these proceedings.
- [18] J. Bartels *et al.*, *Eur. Phys. J.* **C7**, 443 (1999).
- [19] K. Golec-Biernat, M. Wüsthoff, *Phys. Rev.* **D59**, 014017 (1999); *Phys. Rev.* **D60**, 114023 (1999); *J. Phys. G* **28**, 1057 (2002).
- [20] G. Ingelman *et al.*, *Phys. Lett.* **B366**, 371 (1996); *Phys. Rev.* **D64**, 114015 (2001); **D67**, 011301 (2003).
- [21] S. Brodsky, *Acta Phys. Pol. B* **36**, 635 (2005) these proceedings.
- [22] K. Goulianos, *Acta Phys. Pol. B* **36**, 689 (2005) these proceedings; Proc. Les Rencontres de Physique de la Valle d'Aoste 2004, La Thuile, Italy, hep-ph/0407035.
- [23] ZEUS Collaboration, contrib. paper 538 to EPS'03, Aachen, Germany; contrib. paper 6-0246 to ICHEP'04, Beijing, China.
- [24] H1 Collaboration, H1-prelim-01-111, contrib. paper 808 to EPS'01, Budapest, Hungaria.
- [25] H1 Collaboration, H1-prelim-01-112, contrib. paper 984 to ICHEP'02, Amsterdam, Netherlands.
- [26] ZEUS Collaboration, *Eur. Phys. J.* **C38**, 43 (2004).
- [27] H1 Collaboration, H1-prelim-02-012, contrib. paper 089 to EPS'03, Aachen, Germany.
- [28] H1 Collaboration, *Nucl. Phys.* **B619**, 3 (2001); ZEUS Collaboration, *Nucl. Phys.* **B637**, 3 (2002); ZEUS Collaboration, *Nucl. Phys.* **B658**, 3 (2003).
- [29] ZEUS Collaboration, *Nucl. Phys.* **B596**, 3 (2001); H1 Collaboration, H1-prelim-01-114, contrib. paper 811 to EPS'01, Budapest, Hungaria.
- [30] ZEUS Collaboration, contrib. paper 824 to ICHEP'02, Amsterdam, Netherlands.
- [31] N. Nikolaev *et al.*, hep-ph/9708290.
- [32] U. D'Alesio, H. Pirner, *Eur. Phys. J.* **A7**, 109 (2000).
- [33] K. Wichmann (ZEUS Collaboration), Proc. of DIS'04, Štrbské Pleso, Slovakia; contrib. paper 6-0248 to ICHEP'04, Beijing, China.
- [34] H1 Collaboration, contributed paper 6-0821 to ICHEP'04, Beijing, China.
- [35] CDF Collaboration, *Phys. Rev. Lett.* **87**, 241802 (2001).
- [36] CDF Collaboration, *Phys. Rev. Lett.* **88**, 151802 (2002).
- [37] CDF Collaboration, *Phys. Rev. Lett.* **85**, 4215 (2000).
- [38] CDF Collaboration, *Phys. Rev. Lett.* **84**, 5043 (2000).
- [39] J. Bartels *et al.*, *Phys. Rev.* **D63**, 074004 (2001).
- [40] M. Arneodo, Hera-LHC workshop (<http://www.desy.de/~heralhc/>), Oct'04.
- [41] H1 Collaboration *Z. Phys.* **C76**, 613 (1997).
- [42] ZEUS Collaboration, *Eur. Phys. J.* **C6**, 43 (1999).

- [43] ZEUS Collaboration, *Eur. Phys. J.* **C1**, 1/2,81 (1998).
- [44] K.Terashi (CDF Collaboration), Proc. of DIS'04 Štrbské Pleso, Slovakia,
- [45] M. Convery (CDF Collaboration), *Acta Phys. Pol. B* **36**, 665 (2005) these proceedings.
- [46] V. Khoze *et al.*, *Eur. Phys. J.* **C26**, 229 (2002).
- [47] A. Kaidalov *et al.*, *Phys. Lett.* **B559**, 235 (2003).
- [48] A. Kaidalov *et al.*, *Phys. Lett.* **B567**, 61 (2003).
- [49] J. Pumplin, *Phys. Rev.* **D8**, 2899 (1973).
- [50] M. Helbich (ZEUS Collaboration), Proc. of DIS'04, Štrbské Pleso, Slovakia; contrib. paper 6-0248 to ICHEP'04, Beijing, China.
- [51] H. Abramowicz, Proc. of PIC'04, Boston, USA.